Temperature dependence in nanoindentation of a metal substrate by a diamondlike tip

Jin-Yuan Hsieh*
Department of Mechanical Engineering, Ming Hsin University of Science and Technology, Hsinchu 304, Taiwan

Shin-Pon Ju†
Department of Mechanical and Electro-Mechanical Engineering, National Sun Yat-sen University, Kaohsiung 804, Taiwan

Shyh-Hong Li‡ and Chi-Chuan Hwang§
Department of Engineering Science, National Cheng Kung University, Tainan 701, Taiwan
(Received 28 November 2003; revised manuscript received 16 August 2004; published 17 November 2004)

In this investigation, we simulated the nanoindentation of a copper substrate by a diamondlike tip, using molecular dynamics method. A series of simulations according to distinct system temperatures were performed to analyze the temperature dependences of some important physical quantities occurring in the indentation. We found that the maximal normal forces on the tip atoms, both the repulsive and the attractive, the elastic modulus of the indentation system and the network done by the tip during the indentation cycle all decrease with increasing system temperature. By these dependences, we then identified the critical temperature for the transition of plastic flow mechanism in the substrate. The evolution of the crystalline structure in the substrate was analyzed by examining the variation of the structure factor, which measures the perfection of the crystalline structure, during the indentation cycle. An important physical quantity is the difference between the equilibrium absolute values of structure factor before and after the indentation, which can be used to measure the permanent deformation in the substrate produced by the indentation. We found that the difference increases with increasing temperature if the system temperature is below the critical temperature.

DOI: 10.1103/PhysRevB.70.195424 PACS number(s): 68.60.Dv, 62.25.+g, 61.50.Ah

I. INTRODUCTION

Nanoindentation of solid thin films has received a continuously increasing attention because of the remarkable advancements of science and technology in recent years. At nano scales, material properties such as elastic modulus, hardness, fracture toughness, and residual stresses of a solid thin film can be measured from the nanoindentation on its surface by implementing scanning tunneling microscopy (STM) and atomic force microscopy (AFM).[1–4] Investigations of the nanoindentation, on the other hand, provide the knowledge of surface contact nanomechanics required in nano scale wear processes, such as those occurring in materials manufacturing processes,[5,6] and nanofabrication technologies such as the newly developing AFM-based data storage technology[7–10] and nanoimprint lithography.[11,12]

Owing to recent advances in algorithms, interatomics potentials, and computational power, theoretical studies of the nanoindentation in principle are accomplished by using the molecular dynamics (MD) method, instead of the classical continuum theories. Nowadays, the MD methods using empirical interatomic potentials can be implemented in simulating large-scale systems of up to ten million atoms.[13,14] Meanwhile, the existing well developed potentials also make the MD method very applicable to simulate a wide variety of materials in the nanoindentation system. In one of the pioneering MD simulations, Landman *et al.*[15] modeled a nickel tip indenting a gold substrate and observed two significant phenomena occurring when the tip is indented to and retracted from the substrate, respectively. One of the phenomena is, in the indentation phase, the jump-to-contact caused by mechanical instabilities at small tip-substrate distance. The other is the formation of a connective neck at the tip-substrate interface, in the retraction phase, due to strong attraction bonding between the tip and the substrate. The same phenomena were also observed in following simulations, e.g., see Refs. 16–19, in which nanoindentations of metal substrates were studied. In particular, the MD simulations of nanoindentation performed in Ref. 16 were presented to interpret the atomic scale energetics, structure, and formation mechanisms of solid and liquid junctions occurring between a solid metal tip and a clean metal surface or between the tip and a liquid film of hexadecane molecules adsorbed on a solid surface. Yan and Komvopoulos[19] presented adiabatic and isothermal simulations to investigate the effect of substrate temperature and reported the results in both cases were in principle identical. Gannepalli and Mallaprada,[20] on the other hand, performed MD simulations to study the evolution of the plastically deformed region during nanoindentation of a covalently bonded material (silicon). Walsh *et al.*[13,14] studied the nanoindentation of a high-temperature ceramic material, silicon nitride, by performing multi-million-atom MD simulations. Instead of imposing constant indentation speeds in the simulations of Refs. 13–20, Yu *et al.*[21] reported the effects of system temperature, tip-substrate bonding, indentation force, and surface orientation on the indentation depth by acting a constant force on the tip in indenting the substrate for each of their simulations.

The MD simulations mentioned above, except those in Ref. 21, either considered the nanoindentation undergone a constant system temperature,[15–17] or assumed the substrate been indented by a rigid tip.[13,14,18–20] To our knowledge, systemic studies of the effect of the system temperature on the nanoindentation in which the thermal motions of the tip at-

oms according to distinct temperatures are considered are rare. In a realistic nanoindentation, however, heat transfer from tip to substrate or reversely, from substrate to tip, occurs whenever they initially possess different temperatures. For example, the AFM-based data storage process is designed to be operated in a situation that high temperature tips are heating while indenting a substrate of relatively low temperature. In this work, we therefore, are intended to deal with the effect of the system temperature on a nanoindentation using the MD method. We will simulate nanoindentations of a metal substrate by a covalently bonded tip. Isothermal processes are employed to simplify the analysis in consideration that the heats generated in the tip and the substrate during the indentation process is quickly dissipated by the thermal baths.[19] That is, in each of our simulations, both the tip and the substrate are imposed at a same system temperature during the process. Therefore, the main difference between the present and the previous studies[13–20] is that the thermal motions of the tip atoms according to the distinct system temperatures are performed in our simulations. By simulating the normal force on the tip atoms during the complete cycles of nanoindentation under distinct system temperatures, we will establish the temperature dependences of the maximal normal forces, both repulsive and attractive, and the network done by the tip through the process. We will also examine the evolutions of the structure factor[22] in the substrate during the cycles of indentation to identify the temperature dependence of the perfection of crystalline structure.

II. SIMULATION METHODOLOGY

In this work we performed simulations of the nanoindentation on a fcc crystalline copper substrate by a covalently bonded carbon tip by which the effect of the system temperature was studied. The positions and velocities of both the tip and the substrate atoms were obtained as functions of time using the MD method. We assumed the heat generated in the system during the indentation process was dissipated by the thermal baths of the tip and the substrate at a high rate that is much faster than the indentation speed. Therefore, in our simulations the nano scale tip and substrate were controlled at the same temperatures during the indentations, i.e., we have considered the indentations as isothermal processes. The responses of the nanoindentation system corresponding to several distinct temperatures were then simulated. The configuration of the simulated tip and substrate is shown in Fig. 1. The atomically sharp tip is composed of 3681 carbon atoms forming a circular-cone-like structure with a diameter of 46.3 Å and height of 16.4 Å. The upper three layers of the tip are fixed, or rigid, layers, while the rest of it was simulated as the thermal control layers used to maintain the tip temperature through the indentation process. The relatively soft substrate consists of 16 000 fcc copper atoms in a finite slab with lateral area 70.5 Å $\times$ 70.5 Å and thickness 34.4 Å. The up-most part of the copper substrate is composed of 16 thermal control layers used to impose the substrate temperature, which is the same as that of the tip. Below the thermal control layers are two free motion layers designed to allow dislocation motions in the deformed substrate. Besides, the bottom of the substrate contains two fixed layers in preventing the substrate from moving along the direction of the indenting force caused by the tip. In the simulations, periodic boundary conditions were imposed in the lateral x and y directions.

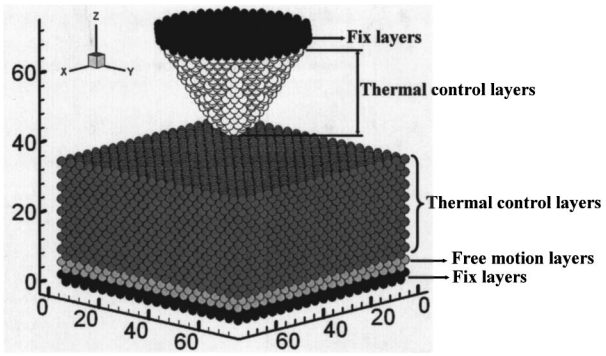

FIG. 1. Configuration of the nanoindentation.

The size of the incremental time step employed in the computations should be smaller than the thermal motion periods of both the tip and the substrate atoms, but it should not be too small since then a large number of time steps is required in the computation which in turn will accumulate a large inevitable computational round-off error. In the present computations, a compromised choice of the time step $\Delta t = 10^{-3}$ ps was thus employed. The MD simulations of nanoindentation comprised equilibrium and indentation stages. In the equilibrium stage, the tip and the substrate were first positioned 10 Å apart in order to avoid the effect of the long-range attractive force between them. Meanwhile, the initial positions of the tip and substrate atoms were prescribed in accordance with their crystalline structures, respectively, and the initial velocities were randomized according to the circumstance temperature using numbers uniformly distributed in an interval. Then, both the tip and the substrate were relaxed to their equilibrium atomic configurations in consequence of the interatomic forces acting on each individual atom. In the second stage of the MD simulation, the indentation was modeled by moving the tip 25 Å downwards at a constant speed ($v = 100$ m/s), and then retracting it back to its original position at the same speed. In both stages, the temperature of the thermal control layers in both the tip and the substrate was controlled at a desired value using rescaling method.[22,23] The leap-Frog algorithm[23] was used to derive the new position and velocity vectors of the tip and the substrate atoms from the corresponding data obtained in the previous step. The motion of each atom in the system was governed by Newton's law of motion in which the resulting force acting on the atom was deduced from energy potential relevant to the interactions with the neighboring atoms within a cut-off radius.

In our simulations, distinct empirical energy potentials appropriate in simulating the carbon-carbon, copper-copper, and copper-carbon bonding were employed, respectively. We used the Tersoff potential[24–27] to simulate the sp^3 covalent bonds among the carbon atoms in the tip. The Tersoff potential, as a function of the atomic coordinates, is given by

TABLE I. Parameters used in the Tersoff potential for carbon-carbon binding.

	C
A	1393.6
B	346.7
λ	3.4867
μ	2.2119
β	1.5724×10^{-7}
n	0.72751
c	38409
d	4.384
h	−0.570 85
R	1.8
S	2.1

$$E=\sum_i E_i=\tfrac{1}{2}\sum_{j\neq i} V_{ij}; \tag{1a}$$

$$V_{ij}=f_c(r_{ij})(A_{ij}e^{-\lambda_{ij}r_{ij}}-B_{ij}e^{-\mu_{ij}r_{ij}}); \tag{1b}$$

$$f_c(r_{ij})=\begin{cases}1, & if\ r_{ij}<R_{ij},\\ \frac{1}{2}-\frac{1}{2}\cos\left(\pi\frac{r_{ij}-R_{ij}}{S_{ij}-R_{ij}}\right), & if\ R_{ij}<r_{ij}<S_{ij}\\ 0, & if\ r_{ij}>S_{ij};\end{cases} \tag{1c}$$

$$b_{ij}=\chi_{ij}(1+\beta_i^{n_i}\xi_{ij}^{n_j})^{-1/2n_i}; \tag{1d}$$

$$\xi_{ij}=\sum_{k\neq i,j} f_c(r_{ik})g(\theta_{ijk}); \tag{1e}$$

$$g(\theta_{ijk})=1+\frac{c_i^2}{d_i^2}-\frac{c_i^2}{d_i^2+(h_i-\cos\theta_{ijk})^2}, \tag{1f}$$

where E is the total energy of all the covalently bonded carbon atoms, E_i is the energy for atom i, V_{ij} is the interaction energy between atoms i and j, r_{ij} is the distance between them, θ_{ijk} is the bond angle between atoms ij and ik, and f_c is a cut-off function to restrict the range of the potential. The values of all the constants appearing in the above equations are listed in Table I.[27] Distinct from the covalently bonded carbon atoms, the copper element of the substrate belongs to the transition metals. In our simulations, the total energy of the metallic bonding in the copper substrate is described by the tight-binding potential[28] given by

$$E=\sum_{i=1}^{N}\left\{Ae^{-p(r_{ij}/r_0-1)}-\left[\sum_j \xi^2 e^{-2q(r_{ij}/r_0-1)}\right]^{1/2}\right\}, \tag{2}$$

where r_{ij} is the distance between copper atoms i and j, r_0 is the first-neighbors distance in the fcc lattice, and the constants $A=0.0855$ (eV), $\xi=1.224$ (eV), $p=10.906$, $q=2.278$ are employed. Although so far there is no specific empirical potentials for simulating the copper-carbon bonding, like the Tersoff potential is for the covalent bonding and the tight-binding potential is for the metallic bonding, we implemented an applicable Morse type pair potential to derive the copper-carbon bonding, The Morse pair reads

TABLE II. Parameter used in the Morse potential for carbon-copper binding.

	Cu−Cu	Cu−C	C−C
D (eV)	0.3429	0.1	2.423
$\alpha(10^{10}\ \mathrm{m}^{-1})$	1.3588	1.7	2.555
$r_0(10^{-10}\ \mathrm{m})$	2.6260	2.2	2.522

$$\phi(r)=D[e^{-2\alpha(r-r_0)}-2e^{\alpha(r-r_0)}], \tag{3}$$

where r is the length of a copper-carbon bond and D, α, and r_0 correspond to the cohesive energy, the elastic modulus, and the atomistic distance at equilibrium, respectively. The appropriate values of D, α, and r_0 are listed in Table II, which had been employed in a nano scale machining research.[29]

III. RESULTS AND DISCUSSION

In this work we performed MD simulations of the nanoindentation on a metal substrate subject to a diamond like tip. The system temperature was taken as the parametric variable in analyzing the thermal effects on the nanoindentation. Several system temperatures employed in this analysis were in between the normal temperature 300 K and a high temperature 1300 K, which is about 100 K below the melting temperature of the copper substrate. But, before showing our main results, we should first discuss the suitability of the present substrate used in our MD simulations. Because of the arrangement of the thermal control layers in both the tip and the substrate, the deformed substrate atoms, while suffering the indentation, can be limited in the zone near around the indenting tip. The size of substrate used in this study, therefore, is sufficiently suitable in analyzing the nonaindentation. The convincible evidence is shown in Fig. 2, in which the results from the employments of the present substrate and a larger one (99.5 Å × 99.5 Å × 45.2 Å) are displayed, respectively. We see that both results in principle are approximately the same.

Only four of the hystereses depicting the variations of the normal force on the tip atoms as functions of the tip-substrate separation distance during the complete cycles of indentation associated with the system temperatures 300, 900, 1000, and 1300 K are shown in Fig. 3, respectively. As can be seen in Fig. 3, in a short interval of time after the tip has begun to move downwards from rest, the negative normal forces indicating the effects of long-range attraction forces between the tip and the substrate atoms were observed. The jump-to-contact phenomenon, which is a universal feature of the surface contact nanomechanics, was observed in each simulation as some of the substrate atoms directly below the tip straining toward the tip atoms. As the tip moved farther to indent into the substrate, the normal

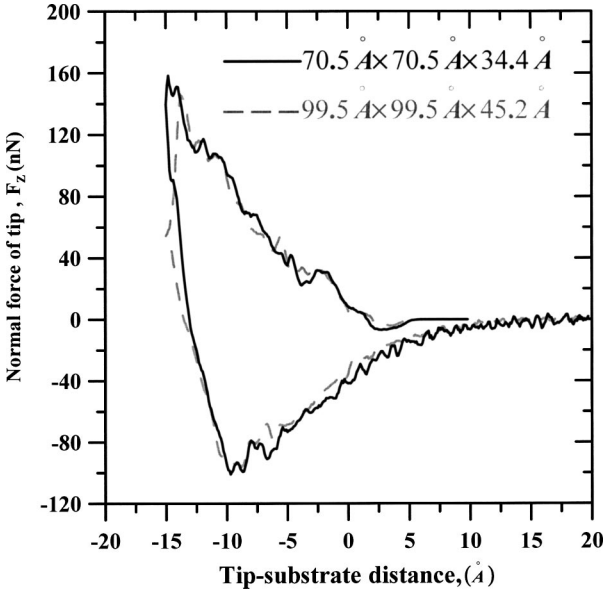

FIG. 2. Variations of the normal force on the tip as functions of the tip-substrate separation distance System temperature is at 300 K. Both the approximately same results are obtained from the simulations employing the substrate of 70.5 Å×70.5 Å×34.4 Å (solid curve) and the substrate of 99.5 Å×99.5 Å×45.2 Å (dashed curve), respectively.

force on the tip atoms gradually changed to become repulsive and increased proportionally, in a sense of average, with the indentation depth. The maximal repulsive force corresponding to each individual system temperature was obtained nearly at the instant when the tip reached the maximal indentation depth, viz., when the tip-substrate separation distance was at −15 Å. It is obvious to find, from Fig. 4, that a

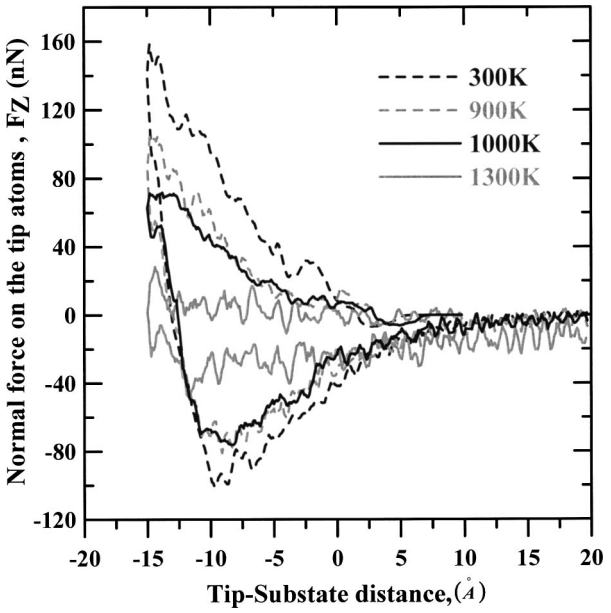

FIG. 3. Variations of the normal force on the tip atoms as functions of the tip-substrate separation distance during the complete cycles of indentation corresponding to 300, 900, 1000, and 1300 K, respectively.

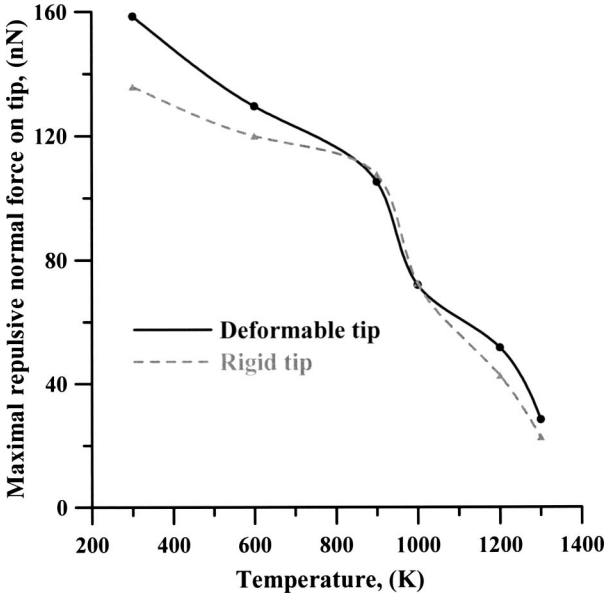

FIG. 4. Temperature dependences of maximal repulsive normal force on the tip atoms in the indentation phase. The solid (dashed) curve represents the result from the assumption of deformable (rigid) tip.

larger maximal repulsive force corresponds to a lower system temperature, since the substrate at a lower temperature is harder to be deformed by the indentation. As shown in Fig. 4, a remarkable reduction of the maximal repulsive force took place when the system temperature was at about 1000 K (actually in between 900 and 1000 K), representing the critical temperature for the transition of plastic flow mechanism.[30] This critical temperature (1000 K) can also be identified in the figures to be presented in what follows.

As the tip has reached the maximal indentation depth, it then was retracted from the substrate at the same rate as in the indentation phase. From Fig. 3, it is observed that at the beginning of the retraction phase, the normal forces on the tip atoms began to vary continuously but quickly from the maximal repulsive to the maximal attractive value in a short range of the tip-substrate separation distance. In this range, the repulsive normal force on the tip atoms obviously is caused by the rebounding response of the elastic substrate, very similar to the reaction of a compressed linear spring after relaxed. However, as the system temperature exceeds the critical 1000 K, the rebounding phenomenon almost disappears because of the plasticity in the substrate. After the repulsion range, the normal force on the tip atoms then became attractive and increased gradually to its maximal value, as the tip kept moving upwards. The variation of the maximal attractive force in the retraction phase as a function of the system temperature was recorded in Fig. 5, showing that the maximal attractive force decreases with increasing system temperature, and also decreases remarkably at about 1000 K. Behind the maximal value, the attractive normal force decreased to zero when the tip was gradually pulled back to its original position. Because the attractive normal force on the tip atoms during the retraction phase was mainly caused by the adhesion between the copper-carbon pairs, the

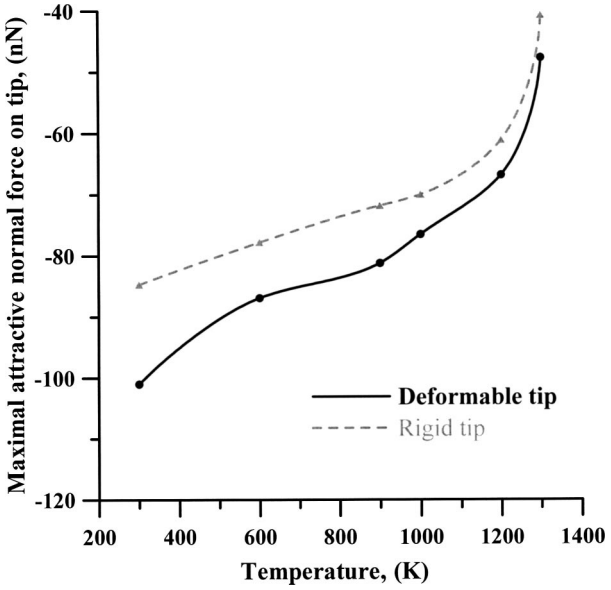

FIG. 5. Temperature dependences of maximal attractive normal force on the tip atoms in the retraction phase. The solid (dashed) curve represents the result from the assumption of deformable (rigid) tip.

decreasing attractive force was due to the fewer copper-carbon bonding occurring when the tip was gradually pulled out of the substrate. In the same interval of time when the gradually decreasing attractive normal force took place, the formation, elongation, and rupture of a connective neck, which is also one of the universal features of the surface contact nanomechanics, were observed. In addition, the variation of effective elastic modulus of the indentation system (the deformable indenter and the substrate) with temperature was shown in Fig. 6 to characterize the elastic behavior in the range between the maximal repulsive and attractive forces. The elastic modulus was estimated using

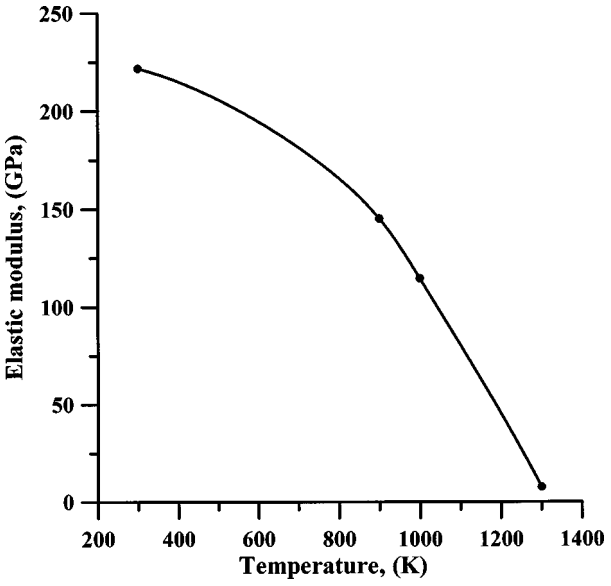

FIG. 6. Temperature dependence of the effective elastic modulus.

the data of the force/distance slope and the projected contact area recorded at the beginning of the retraction phase by the same way adopted in relevant researches; e.g., see Refs. 31 and 32. It is observed that the elastic modulus decreases with increasing temperature and decreases remarkably when the temperature exceeds about 1000 K. It should be noticed that the elastic modulus at 300 K presented here ($\sim$220 GPa) is about 146% of that obtained in a previous experimental study $\sim$150 GPa.[33] Such discrepancy is mainly due to the high strain rate employed in the MD simulation, the employment of the fixed layers at the bottom of the substrate and the effect of the surface energy generated in the indentation on the elastic modulus.[32] Although a more complete interpretation of the role changes in the elastic modulus played in the plastic structure of the indented system requires future studies, the variation of the elastic modulus with temperature shown in Fig. 6 is also helpful for identifying the critical temperature for the transition of plastic flow mechanism.

It should be mentioned here that, because of the effect of the rather high indentation speed employed in the present simulations, the hystereses shown in Fig. 3, are not like those shown in Ref. 19, in which low indentation speeds were applied. In the simulations of Ref. 19, the indentation speeds corresponding to the figures shown therein were in between $v=5-10$ m/s, so the atom reconstructions in the substrate can develop in time to decrease the normal force on the tip atoms behind the compressive yield force and then harden the substrate, in the indentation phase, and cause the saw-tooth like patterns behind the maximal attractive normal force, in the interval of the formation and elongation of the connective neck. In our simulations, however, the high indentation speed ($v=100$ m/s) caused the atom reconstructions unable to develop fully in time and, therefore, the yielding and saw-tooth phenomena were not observed, but the hystereses shown in this work are like those shown in Ref. 17, in which the indentation speed was at $v=139$ m/s. Moreover, effects of the high strain rate produced by the indentation speed of 100 m/s indeed will lead to over-estimated strengths, especially when system temperature is low. The over-estimations, however, will reduce with increasing temperature. As a result, the effect of the high strain rate does not qualitatively affect the temperature dependences shown in Figs. 4–6, nor does it affect the quantitative estimation of the critical temperature for the transition of plastic flow mechanism.

The plastic deformation occurring in the indented substrate can be alternatively interpreted by the evolution of dislocation. Dislocation motions can be easily observed when temperature is low, for example, Zhu *et al.*[34] has considered the dislocation motions in two-dimensional (2D) and three-dimensional (3D) nanoindentations at 1 K. The lowest temperature considered in this study was 300 K, so we will only display the dislocation motion occurring in the substrate at this temperature. Since the MD method has the advantage of allowing defects to nucleate and evolve spontaneously, the atomic structure of the emerging dislocation is directly revealed by the method. In Fig. 7, we show the snapshots of atomic structure in the substrate during the indentation at 300 K. In this figure, only the back half of the substrate is shown and the substrate atoms are gray-scaled by coordinate

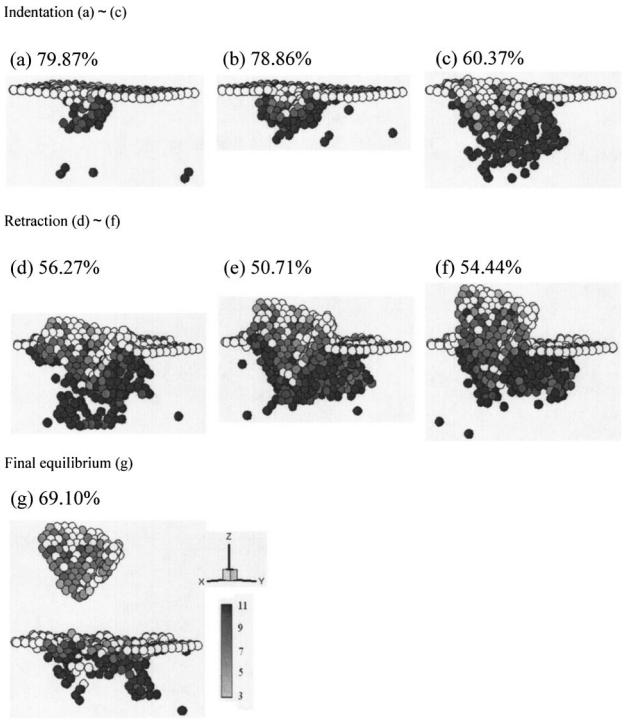

FIG. 7. Snapshots showing atomic structures in the substrate undergoing the indentation at 300 K. The snapshots are taken when the tip-substrate distances at (a) −2.5 Å (b) −5 Å, (c) −15 Å, in the indentation phase, and (d) −10 Å, (e) −5 Å, and (f) 0 Å in the retraction phase, respectively. Snapshot (g) shows the final equilibrium of the substrate, and the atoms above the substrate represent those attached to the indenter. In each snapshot, the perfectly coordinated atoms are removed but their percentage in the substrate is shown, and the imperfectly coordinated atoms are grey-scaled in the way that darker atoms have larger coordinate numbers. The white atoms are those initially placed at the surface.

number[35] N. The perfectly coordinated atoms ($N=12$) have been removed from the snapshots for clarity, such that only surface and imperfectly coordinated atoms are visible. We notice that at the beginning of the indentation, the dislocation embryo, while suffering thermal diffusion at the same time, is consistent with the configuration of the indenter and similar to the one shown in the 3D simulation of Zhu *et al.*.[34] Moreover, we also show in each of the snapshots the percentage of the perfectly coordinated atoms in the substrate. It is shown that the percentage is always greater than about 50%, as the substrate is suffering the indentation, also indicating that the present substrate used in our simulations is suitable.

By the hysteresis of the normal force on the tip atoms, we are able to deduce the total work done by the tip causing deformations in the substrate through the complete cycle of a nanoindentation. As schematically depicted in Fig. 8, in the indentation phase, a negligible negative work(area I) is done by the tip corresponding to the long-range attractive force between the tip and the substrate and a positive work (area II+area III) then is done by the tip corresponding to the repulsive normal force on the tip atoms. In the retraction phase, a negative work (area III) is done by the tip due to the rebounding reaction of the elastic substrate at the beginning of the phase and afterwards a positive work (area IV

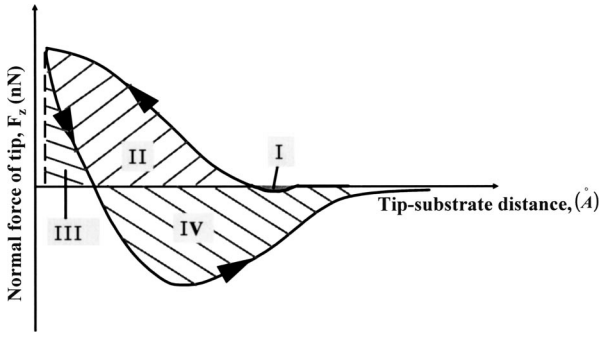

FIG. 8. Schematic depiction of the work done by the tip during an indentation cycle. Detail descriptions of the areas I, II, III, and IV, respectively, can be found in the context.

+area I) is done by the tip eventually due to the attractive normal force while the tip is moving upwards. So, the total net work done by the tip can be estimated by computing the area enveloped in the hysteresis cycle of an indentation process (area II+area IV). The variations of the total net works done by the tip as functions of the system temperature are shown in Fig. 9. Reading Fig. 9, one realizes that the applied work by the tip during the complete process will decrease with increasing system temperature. In Fig. 9, and Figs. 4 and 5 as well, the solid curves correspond to the results of the simulations in which the tip was deformable due to the thermal motions of the tip atoms, while the dashed curves, on the other hand, represent the results of the simulations in which the tip was assumed to be rigid. We can see that, from Figs. 4, 5, and 9, when the system temperature is relatively low, the differences between both results can be remarkable; these remarkable differences explain why in this work we have modeled the deformable tip to obtain more accurate results.

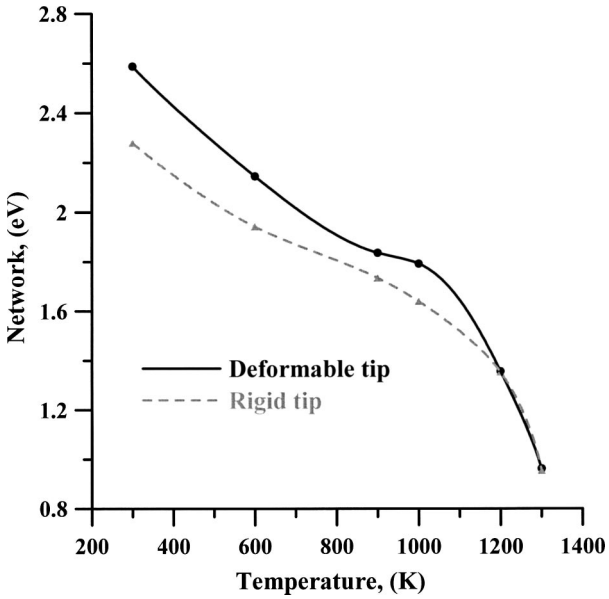

FIG. 9. Temperature dependences of the network done by the tip through indentation cycles. The solid (dashed) curve represents the result from the assumption of deformable (rigid) tip.

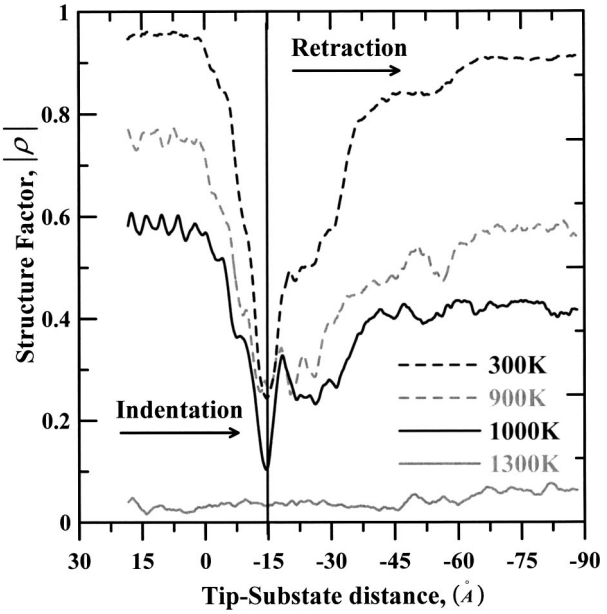

FIG. 10. Variations of the absolute values of structure factor in the substrate, as functions of the tip-substrate separation distance. Corresponding to the variations, the system temperatures are 300, 900, 1000, and 1300 K, respectively.

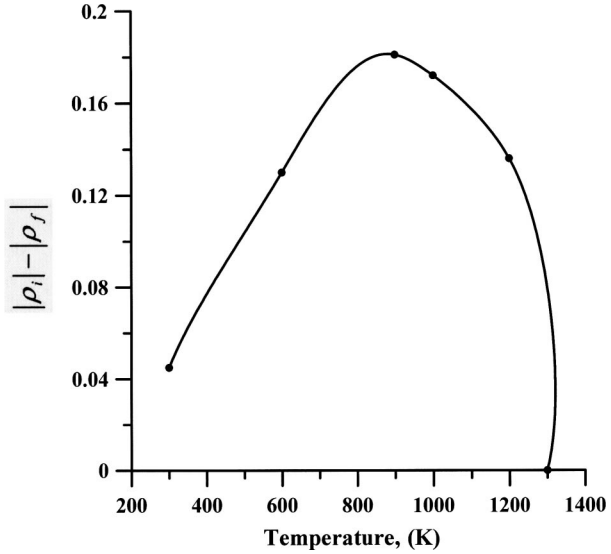

FIG. 11. Temperature dependence of the difference between the equilibriums of the absolute structure factors before and after the indentation.

The normal force on the tip atoms in turn exerted on the substrate atoms simultaneously and caused them to dislocate from their previous positions from time to time. The complex analysis of the variation of the substrate lattice structure, when the substrate was suffering the indentation cycle, can be simplified by examining the evolution of the structure factor for the copper substrate, defined by Ref. 22,

$$\rho = \frac{1}{N_a} \sum_{j=1}^{N_a} \exp(i\vec{k} \bullet \vec{j});$$

$$\vec{k} = \frac{2\pi}{a}(1,-1,1), \tag{4}$$

where Na is the number of the selected atoms in the deformation zone around the tip, r_j represents the position vector of atom j, and a is the length of the unit fcc lattice in the copper substrate. When the structure factor defined by (4) is employed in the analysis, a perfect fcc lattice structure is identified if $|\rho|=1$, while, on the contrast, a completely disordered liquid-like structure will correspond to $|\rho|=1/\sqrt{Na}$, i.e., a higher absolute value of the structure factor represents a more perfect lattice structure in the solid substrate. The evolutions of the structure factor as functions of time during the complete cycles of indentation were recorded and those corresponding to the system temperatures 300, 900, 1000, and 1300 K were shown in Fig. 10, respectively. In this figure, the temporal variable has been transformed to the tip-substrate separation distance. From Fig. 10, it was rationally observed that before the indentations were begun with, the absolute values of structure factor were maintained at their initial equilibriums, which will decrease with increasing temperature. In the indentation phase, the absolute values of structure factor all reduced to their minimums, as shown in the figure, after the tip had reached its maximal indentation depth. This minimal value will almost be the same when the system temperature is below the critical temperature, but will reduce remarkably as the system temperature exceeds the critical point. Meanwhile, the minimal absolute value of the structure factor tends to last longer with higher system temperature. Then, in the retraction phase, the absolute value of the structure factor increased as the tip was gradually pulled out of the substrate and eventually became its final equilibrium value, which will also decrease with increasing temperature. Notice that when the system temperature is close to the melting point, as shown by the variation associated with 1300 K in Fig. 10, the absolute value of the structure factor in fact maintains the same during the complete cycle of the indentation since then the substrate is almost totally plastic. The permanent deformation in the elastic substrate (i.e., as the substrate possesses a temperature below the critical point), under the indentation, therefore can be measured by the difference between the initial and the final absolute values of the equilibrium structure factors. The results of the simulations showed that the difference of the absolute values of structure factor in the substrate before and after the indentation depends on the system temperature, and the dependence is shown in Fig. 11. Interestingly, we found, from Fig. 11, that when the system temperature was below the critical temperature for the transition of plastic flow in the substrate, viz., about 1000 K, the difference between the initial and the final absolute values of the equilibrium structure factors increased with increasing system temperature, while as the system temperature is higher than the critical temperature the difference, on the contrast, dropped remarkably with increasing temperature, since a substrate at the higher temperature was already plastic before the indentation. It, therefore, should be noticed that as long as the nanoindentation is accomplished under a temperature below the critical temperature for a plastic substrate, the complete process will require

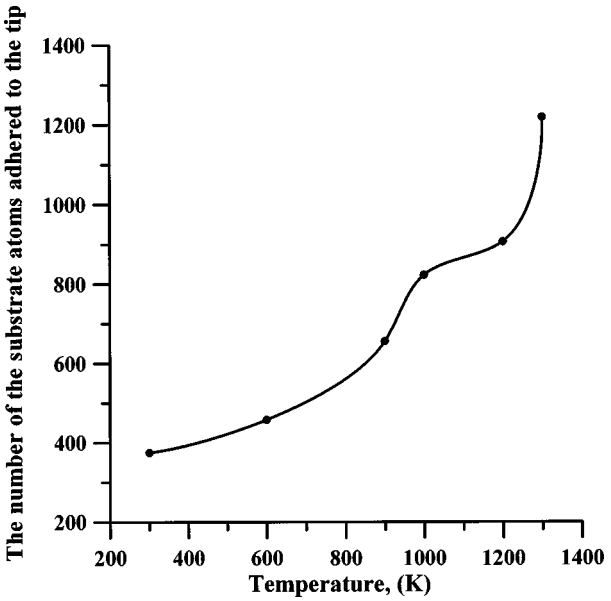

FIG. 12. Temperature dependence of the number of the substrate atoms adhered to the tip.

a smaller work by the tip while leave a more remarkable permanent deformation in the substrate if the system is maintained at a higher temperature. This phenomenon is crucially important to the nanomechanism implemented in the nanofabrication technologies such as the AFM-based data storage and the nanoimprint lithography, in which a polymethylmethacrylate (PMMA) layer is designed to be indented by arrayed heated tips, in the former, and stamped by a heated mold, in the latter case, respectively, so that nanoscale features with high resolutions can be permanently produced in the substrate. Although the present substrate material is not the same as that employed in the mentioned nanofabrications, the present results are qualitatively valuable to the design of the fabricating specifications required in these processes. The trend that below the critical temperature the difference of the equilibrium structure factors will increase with increasing temperature can also be checked by observing the consistent temperature dependence of the number of the substrate atoms adhered to the tip after the nanoindentation is finished. In Fig. 12, we observe that the number of the adhered copper atoms to the tip increased with increasing system temperature, resulting in a larger permanent nanoasperity on the substrate surface.

IV. CONCLUSION

We have performed simulations of the nanoindentation of a copper substrate subject to a diamondlike tip, using the MD method. In each of the present simulations both the tip and the substrate were assumed at a same system temperature in the complete indentation cycle. The system temperature was the parametric variable in the present simulations employed to analyze the thermal effects on the nanoindentation. By the MD simulations, we have in this work identified the critical temperature for the transition of plastic flow mechanism in the copper substrate, like Yan and Komvopoulos[19] have done for the fcc crystalline substrate in their work. To summarize, the thermal effects include:

I. The maximal repulsive normal force on the tip atoms, in the indentation phase, will decrease with increasing temperature;

II. the maximal attractive normal force on the tip atoms, in the retraction phase, also decreases with increasing temperature;

III. the effective elastic modulus of the indentation system decreases with increasing temperature; however, a complete answer regarding the role of elastic modulus changes plays in the structure parameter requires future studies;

IV. when the system temperature is below the critical temperature for the transition of plastic flow in the substrate, the total network done by the tip through the complete cycle of an indentation will decrease with increasing temperature;

V. when the system temperature is below the critical point, a more significant permanent deformation will be produced in the substrate subject to a higher temperature.

The last two effects of the system temperature are significantly important to the nanomechanism involved in nanofabrication processes, for example, the AFM-based data storage and the nanoimprint lithography technologies. These trends qualitatively interpret the utility of heated array of tips in indenting or a heated mold in stamping a relatively soft substrate in the nanofabrications. Qualitatively, more accurate MD simulations for these nanofabrication processes should be accomplished by employing suitable empirical potentials to model the interactions among the particles in the PMMA substrate and between the tip and the substrate atoms. But this is not the main issue to be concerned within this work.

ACKNOWLEDGMENTS

The authors gratefully acknowledge the financial support to this research by the National Science Council, Taiwan, under Grant Nos. NSC 92/2511-S-006-010, NSC 92-2212-E-006-066, and NSC 92-2212-E-159-001.

*Email address: jyhsieh@mail.must.edu.tw
†Email address: jushin-pon@mail.nsysu.edu.tw
‡Email address: nckues2002@pchome.com.tw
§Author to whom correspondence should be addressed. Email address: chchwang@mail.ncku.edu.tw

[1] H. Ichimura and I. Ando, Surf. Coat. Technol. **145**, 88 (2001).
[2] A. A. Volinsky, J. B. Vella, and W. W. Gerberich, Thin Solid Films **429**, 201 (2003).
[3] S. Sundararajan and B. Bhushan, Sens. Actuators, A **101**, 338 (2002).
[4] H. C. Barshilia and K. S. Rajam, Surf. Coat. Technol. **155**, 195 (2002).

[5] C. C. Hwang, R. F. Fung, and J. S. Lin, J. Sound Vib. **203**, 363 (1997).
[6] T. H. Fang, C. I Weng, J. G. Chang, and C. C. Hwang, Thin Solid Films **396**, 166 (2001).
[7] P. Vetriger, J. Brugger, M. Despont, U. Drechsler, U. Durig, W. Haberle, M. Lutwyche, H. Rothuizen, R. Stutz, R. Widmer, and G. Binnig, Microelectron. Eng. **46**, 11 (1999).
[8] G. Binnig, M. Despont, U. Drechsler, W. Haberle, M. Lutwyche, and P. Vetriger, Appl. Phys. Lett. **74**, 1329 (1999).
[9] M. Despont, J. Brugger, U. Drechsler, W. Haberle, M. Lutwyche, H. Rothuizen, R. Stutz, R. Widmer, G. Binnig, H. Rohrer, and P. Vetriger, Sens. Actuators, A **80**, 100 (2000).
[10] P. Vetriger, M. Despont, U. Drechsler, U. Durig, W. Haberle, M. Lutwyche, H. Rothuizen, R. Stutz, R. Widmer, and G. Binnig, IBM J. Res. Dev. **44**, 323 (2000).
[11] S. Y. Chou, P. R. Krauss, and P. J. Renstrom, Science **272**, 85 (1996).
[12] S. Zankovych, T. Hoffmann, J. Seekamp, J.-U. Bruch, and C. M. S. Torres, Nanotechnology **12**, 91 (2001).
[13] P. Walsh, R. K. Kalia, A. Nakano, and P. Vashishta, Appl. Phys. Lett. **77**, 4332 (2000).
[14] P. Walsh, A. Omeltchenko, R. K. Kalia, A. Nakano, and P. Vashishta, Appl. Phys. Lett. **82**, 118 (2003).
[15] U. Landman, W. D. Luedtke, N. A. Burnham, and R. J. Colton, Science **248**, 454 (1990).
[16] U. Landman, W. D. Luedtke, J. Ouyang, and T. K. Zia, Jpn. J. Appl. Phys., Part 1 **32**, 1444 (1993).
[17] H. Rafii-Tabar and Y. Kawazon, Jpn. J. Appl. Phys., Part 1 **32**, 1394 (1993).
[18] K. Komvopoulos and W. Yan, J. Appl. Phys. **82**, 4823 (1997).
[19] W. Yan and K. Komvopoulos, Trans. ASME, J. Tribol. **120**, 358 (1998).
[20] A. Gannepalli and S. K. Mallapragada, Nanotechnology **12**, 250 (2001).
[21] H. Yu, J. B. Adams, and L. G. Hector, Jr., Modell. Simul. Mater. Sci. Eng. **10**, 319 (2002).
[22] D. C. Rapaport, *The Art of Molecular Dynamics Simulation* (Cambridge University Press, Landon, 1997).
[23] D. Frenkel and B. Smit, *Understanding Molecular Simulation* (Academic, San Diego, 1996).
[24] J. Tersoff, Phys. Rev. Lett. **56**, 632 (1986).
[25] J. Tersoff, Phys. Rev. B **37**, 6991 (1988).
[26] J. Tersoff, Phys. Rev. B **38**, 9902 (1988).
[27] J. Tersoff, Phys. Rev. B **39**, 5566 (1989).
[28] F. Cleri and V. Rosato, Phys. Rev. B **48**, 22 (1993).
[29] K. Maekawa and A. Itoh, Wear **188**, 115 (1995).
[30] R. W. Hertzberg, *Deformation and Fracture Mechanics of Engineering Materials* (Wiley, New York, 1989).
[31] W. C. Oliver and G. M. Pharr, J. Mater. Res. **7**, 1564 (1992).
[32] Y. Isono and T. Tanaka, JSME Int. J., Ser. A **42**, 158 (1999).
[33] J. M. Antunes, A. Cavaleiro, L. F. Menezes, M. I. Simões, and J. V. Fernandes, Surf. Coat. Technol. **149**, 27 (2002).
[34] T. Zhu, J. Li, K. J. Van Vliet KJ, S. Ogata, S. Yip, and S. Suresh, J. Mech. Phys. Solids **52**, 691 (2004).
[35] Ju Li, Modell. Simul. Mater. Sci. Eng. **11**, 173 (2003).